# GNSS–Camera Systems for Heritage Documentation. Accuracy assessment of measurements of inaccessible points and preliminary tests in photogrammetric applications

# GNSS–Camera Systems for Heritage Documentation. Accuracy assessment of measurements of inaccessible points and preliminary tests in photogrammetric applications.

Lorenzo Teppati Losè [1], Filiberto Chiabrando[1], Fabio Giulio Tonolo[1]

[1] LabG4CH, Department of Architecture and Design (DAD) - Politecnico di Torino, Viale Mattioli 39, 10125 Torino (Italy) – lorenzo.teppati@polito.it, filiberto.chiabrando@polito.it, fabio.giuliotonolo@polito.it

**Keywords:** GNSS-camera system, Photogrammetry, Accuracy assessment, Inaccessible Points, Built Heritage.

**Abstract**

The measurement of Ground Control Points is a crucial but time-consuming step in photogrammetric surveys, especially in the Built Heritage domain. This study investigates the use of a new generation Global Navigation Satellite System receiver equipped with an integrated camera to measure inaccessible points (to be used as GCPs, e.g. on building façades), combining satellite positioning and photogrammetry in a single device. The approach was tested on a historical building using both the tested GNSS-camera system and traditional Total Station topographic measurements as reference. Results show that the proposed method can achieve centimetric accuracy, with horizontal and vertical errors of about 3-5 cm (in line with the adopted NRTK service). While a small systematic shift was observed, the overall geometric consistency of the measured points remained within acceptable limits for many heritage documentation applications. Additionally, the georeferenced images acquired by the system were successfully used in a Structure from Motion (SfM) direct georeferencing workflow, producing 3D models and orthophotos with good metric reliability when compared to other data, such as TLS scans. The study demonstrates that GNSS-camera systems can significantly reduce fieldwork time while providing reliable spatial data, representing a promising solution to be integrated into heritage documentation pipelines in an efficient and flexible way.

## 1. Introduction

Among the different phases of the survey process, the one related to the measurement of Ground Control Points or Check Points ((G)CPs), and the possible positioning of artificial markers if required, is still the one demanding a considerable effort.

This step is considered the most time-consuming among the tasks to be carried out by the surveyors in the field (Remondino & Campana, 2014; Seo et al., 2024). (G)CPs can be placed using artificial targets (including coded ones) or simply be represented by visible and sharp details of the objects of the survey (natural points). Traditional topographic techniques are generally used to measure (G)CPs in the field, such as side shot measurements with a Total Station (TS) or acquisition with a Global Navigation Satellite System (GNSS) receiver using different configurations. In the last decade, the evolution of the latter, combined with a wider availability of Continuously Operating Reference Stations (CORS) infrastructures, allowed a rapid diffusion of Network Real Time Kinematic (NRTK) approaches that became prominent for the measurement of (G)CPs with 3-5 cm accuracy in outdoor scenarios (Forlani et al., 2018; Štroner et al., 2020; Tomaštík et al., 2019).

When data acquisition is performed by means of Uncrewed Aerial Systems (UAS), the synergy between NRTK approaches and these aerial platforms is particularly evident (Agüera-Vega et al., 2017; Bolkas, 2019; Rangel et al., 2018).

These GNSS-based solutions enable rapid acquisition of (G)CPs in the field with positional accuracy compliant with the requirements of most applications (e.g., architecture, engineering, urban planning, environmental monitoring, etc.). Adopting NRTK approaches requires internet connectivity in the field, access to an NRTK correction service, and compatible GNSS equipment.

Nevertheless, a major limitation of these approaches is the inability to measure targets not on the ground, thereby limiting the ability to measure inaccessible points, e.g. details on vertical surfaces. In the domain of the Built Heritage survey, these limitations are particularly evident. When dealing with buildings and structures, the placement and homogeneous distribution of (G)CPs, also on vertical facades, is even more crucial to properly manage and document the elevation component of these architectural objects.

This issue is generally overcome by adopting side-shot measurements via TS. This approach guarantees a complete coverage of all the features of the surveyed site, but is limited in terms of cost-effectiveness ratio if compared to NRTK approaches. This limitation is primarily related to the additional time required in the field to complete the measurements phase of (G)CPs and to the increased level of expertise required to use a TS and process the related measurements.

In recent times, a potential solution to this issue has emerged from the combination of digital photogrammetry, Inertial Measurement Unit (IMU) and satellite observation in the latest GNSS receivers available on the market. These new-generation instruments combine one or more calibrated cameras with the GNSS antenna and the IMU (to estimate the camera attitude) and allow the measurement of (G)CPs of inaccessible points. The aim of this contribution is to test the precision of these approaches and evaluate if, and how, they can be integrated into the overall survey process of Built Heritage, with a focus on photogrammetric workflows.

## 2. Materials and methods

### 2.1 The tested GNSS solution: Stonex S999 GNSS receiver

The instrument tested in this work is the Stonex S999 GNSS receiver (Figure 1). This receiver is equipped with 1408 multi-constellation channels. It features a 4G modem, a UHF radio and an Inertial Measurement Unit (IMU).

The receiver is also equipped with two different cameras: a frontal one for photogrammetric applications and a camera located at the bottom of the receiver for stakeout applications. The main specifications of the instruments are reported in Table 1.


Figure 1. Stonex s999 GNSS receiver (https://www.stonex.it/).

| | | |
|---|---|---|
| Satellite signal tracked | GPS, GLONASS, BEIDOU, GALILEO, QZSS, IRNSS, SBAS | |
| Channels | 1408 | |
| Tilt Range | 0-60° | |
| N-RTK positioning | Fixed RTK Hz: 5 mm +0.5 PPM RMS | Fixed RTK Vz: 10 mm +0.5 PPM RMS |
| Lower Camera | 2MP, Image frame rate: 30 frame/s, FoV 72° | |
| Frontal Camera | 2MP, Image frame rate: 5 frame/s, Video frame rate: 30 frame/s, FoV 88° | |
| RTK + IMU | 5 mm + 0.7mm/° of tilt | |

Table 1. Stonex S999 main specifications.

In addition to the traditional features of a GNSS survey-grade receiver, the S999 integrates some photogrammetric-based solutions. In this contribution, we will focus solely on applications related to the receiver's frontal camera.

The receiver's frontal camera, through the use of the connected software Stonex Cube-a (v.6.4.7), can be used to measure points that are physically inaccessible to the receiver. For example, this feature can be used to measure ground points in an inaccessible area that is visible from the receiver's camera. More importantly for the Built Heritage documentation, the use of the frontal camera enables the measurement of points on vertical surfaces, such as building facades.

The GNSS photogrammetry-based solution (GNSS-Ph) can be used in NRTK mode once a fixed solution for the receiver's position is achieved. The camera is calibrated by Stonex, and it is used to capture a video of the area of interest. The instrument's tilt, as well as the camera attitude, is also taken into account thanks to the IMU unit embedded in the receiver.

Frames are later extracted from the video and used to measure the coordinates of points selected by the operator by means of digital photogrammetric processes (details are not disclosed by the company). There are, of course, some constraints, such as lighting conditions, object texture, and sensor/object distance, that are typical of photogrammetric applications and that need to be considered as well in this scenario.

### 2.2 Research goals

This contribution addresses two main topics related to the use of the S999 and similar solutions in the domain of Built Heritage documentation.

The first part of the work evaluates the accuracy of the (G)CPs measurements extracted via the GNSS-Ph. Some (G)CPs have been measured in ad hoc test scenarios on the façades of historical buildings, adopting both traditional topographic techniques (forward intersection – using a georeferenced first-order control network) and the GNSS photogrammetric solution. The measurements obtained using the two approaches are then compared and evaluated to validate the accuracy of the GNSS photogrammetric approach. Both coordinates and 3D Euclidean distances are compared among the reference datasets and the measured ones. The operative constraints of adopting this solution, as well as its possible limitations, are presented and discussed.

The second part of the work concerns the use of data acquired by the GNSS camera within a standard Structure from Motion (SfM) approach. Several aspects are considered in this part of the work. The images (frame extracted from the video acquired by the receiver) are downloaded by the GNSS and are georeferenced, and can thus be used to exploit direct georeferencing approaches.

At the time of writing, unfortunately, due to the controller's software still being in development and continuously updated, the attitude for the acquired images could not be exported from the GNSS software and thus needs to be re-estimated during photogrammetric processing.

The first research question for this part of the work is thus related to the precision of the geotag associated with these images and whether a direct georeferencing approach can be successfully achieved (Teppati Losè et al., 2023).

The second question is related to the overall quality of the 3D model generated from these images, in terms of metric, geometric, and radiometric quality. Issues related to camera resolution and camera calibration will be addressed as well. The processing of the acquired images will be carried out using commercial software solutions.

To evaluate and validate these approaches, independently measured (G)CPs will be used, along with 3D reference data acquired through other techniques that produce higher-resolution, more accurate point clouds (in our case, LiDAR).

## 3. Test setup

To evaluate and analyse the performance of the GNSS photogrammetric approach, an ad hoc test field in a relevant heritage site was used: the Castello del Valentino in Torino, Italy (Figure 2).

This castle is a remarkable example of architectural heritage located in Turin (Piedmont, Italy). It was built in the 16th century and became the residence of the House of Savoy in 1564, when Emanuele Filiberto moved the capital to Turin and acquired the building. In the 17th century, Cristina of France promoted the transformation of the palace into a maison de *plaisance* following the French model; during this phase, the architects Carlo and Amedeo di Castellamonte designed a major expansion that doubled the existing structure, giving the building its current monumental appearance. At the beginning of the 19th century, no longer used as a ducal residence, the building housed the Veterinary School and was later used as military barracks until it was transferred from the Crown to state ownership in 1850. Since the late 1940s, the building has been owned by the Politecnico di Torino and currently hosts the Department of Architecture and Design (DAD) and the Inter-university Department of Regional & Urban Studies and Planning (DIST).

Figure 2. The Castello del Valentino (https://castellodelvalentino.polito.it/ )

In the area, a first-order control network was set up, measured and updated over the last decades in the main courtyard of Castello del Valentino. The first-order control network was also measured by means of static GNSS acquisitions, and all the vertices are thus georeferenced in the EPSG:32632 - WGS 84 / UTM zone 32N coordinate system.

For the test relevant to this contest, it was decided to focus on the southern wing of the castle and, more specifically, on the façade facing the courtyard; two vertices of the first-order control network were used for the TS measurements (Figure 3).

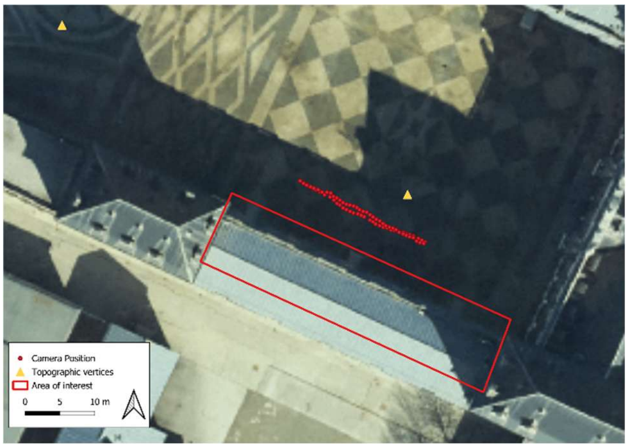


(a)

b)

Figure 3. The portion of the Castello del Valentino selected for the tests, including the control network topographic vertices (a) and the façade surveyed with the GNSS-Ph system (b)

This façade was the object of the subsequent field measurements. In the first place, 20 points were measured with TS, selecting natural features of the façade (Figure 4).

It was decided to work with natural features rather than coded targets to simulate the most challenging scenario of heritage recording, when, due to the fragility of the asset, it is not possible to place coded targets on the surfaces of interest to the survey. This is quite a common situation when dealing with the documentation of precious and fragile assets, and we wanted to test the performance of the GNSS photogrammetric approach and the overall data acquisition and processing pipeline in this specific situation, to see whether it can support the operators involved in the process.

The ground control points on the façade were measured via a traditional Total Station topographic approach with a side-shot survey using the vertices of the first-order control network available in the Castello. This operation allowed us to acquire the coordinates of the ground control points independently from the one with the GNSS-Ph solution provided by the receiver (Figure 6). As shown in Figure 4, the points are homogeneously distributed on the portion of the façade acquired using the GNSS.

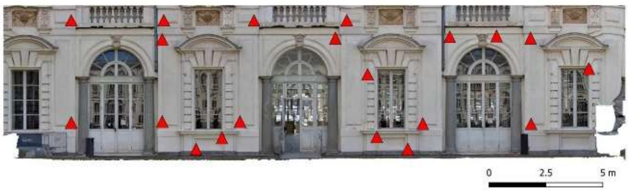


Figure 4. Position (red triangles) and distribution of points measured with the TS on the façade of interest

The second phase of the acquisition campaign was dedicated to the GNSS photogrammetric acquisition with the Stonex S999. The operation is managed by the controller connected to the instrument, which provides a real-time display of the camera and overall control of the operation. To complete the acquisition, some requirements must be respected:

1. A fixed solution of the RTK. In our case a NRTK approach was used, exploiting the real-time corrections downloadable from the CORS network of the Lombardia, Piemonte, and Valle d’Aosta regions (https://www.spingnss.it/)

2. Wi-Fi connection between the receiver and the controller must be ensured
3. The tilt correction function should be enabled

Figure 5. Example of data acquisition with the Stonex S999 for the GNSS-Ph approach

Once the instrument's setup is complete, the acquisition can proceed. The operator can move freely while the receiver is installed on the surveying pole (Figure 5), aiming the GNSS camera at the façade of interest. The operator must ensure consistency in the camera alignment toward the façade during acquisition, while the images are acquired based on a pre-analysis of surface features generated by the software. The software ensures sufficient overlap between images and allows the acquisition of a maximum of 100 images per acquisition session. In our case, the acquisition lasted 3 minutes and resulted in a total of 71 acquired images.

Once the acquisition is complete, the coordinates of the point of interest can be measured and extracted directly from the controller (Figure 6). In our case, images were acquired at an average distance of 7.4 meters from the façade (expected Ground Sample Distance – GSD below 1 cm), with a first acquisition with the receiver at an average height of 2 meters from the ground, and a second acquisition following the same path as the first (backwards) at an average height of 2.4 meters. This acquisition strategy was used to acquire a larger portion of the façade at the higher level. The same approximate orientation was maintained for both acquisitions, with the camera main axis perpendicular to the façade.

After the acquisition, it is possible to select an image and measure the point coordinates through the app interface (Stonex Cube-a v.6.4.7). A crosshair can be placed on the point of interest to query its coordinates. If the measurement is successful, the coordinates are returned together with the Root Mean Square (RMS) error for the northing, westing, and height components.

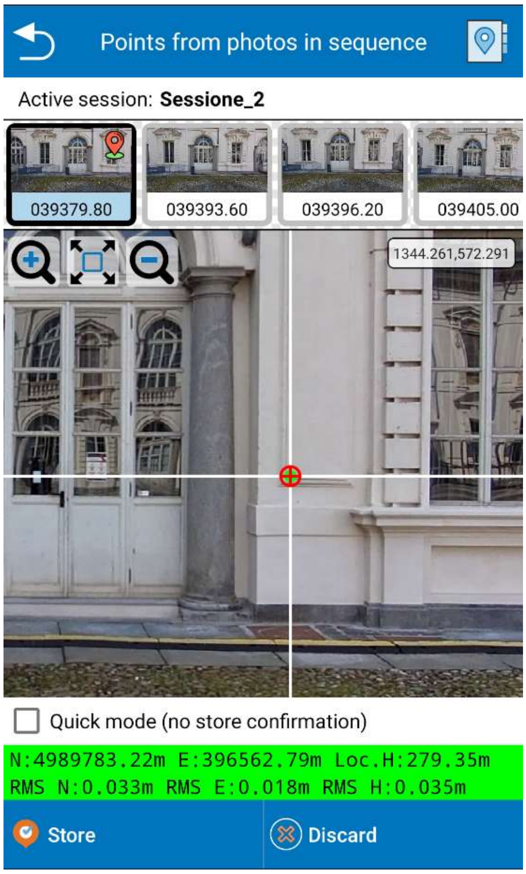


Figure 6. The controller interface for the point measurements using the images acquired by the GNSS camera

## 4. Data analyses

Three main analyses were completed on the data acquired and processed with the Stonex S999: the assessment of the accuracy of G(CPs), an evaluation of the potential of the acquired images for an SfM approach, and a final evaluation of the generated added-value metric products.

### 4.1 Accuracy assessment of inaccessible points measured with GNSS-Ph

The first analysis completed was related to the comparison between the coordinates measured via traditional topographic approaches and those measured via the GNSS embedded photogrammetric approach (GNSS-Ph), which exploits the camera, the IMU and the NRTK centimetric positioning.

A set of 20 points was surveyed twice: first by GNSS-Ph, for which the acquisition software automatically provided horizontal root mean square error (HRMS) and vertical root mean square error (VRMS), and then by total station (TS), used as the ground reference technique. Because the TS survey was performed with sub-centimetric precision, TS coordinates were used as reference values in the accuracy assessment.

The global RMSE estimated automatically by the GNSS-Ph software are:

GNSS-Ph estimated global HRMSE = 0.034 m
GNSS-Ph estimated global VRMSE = 0.034 m

For each point, the GNSS coordinates were compared with the corresponding TS coordinates.

Signed residuals ($\Delta E_i$, $\Delta N_i$, $\Delta H_i$) were computed separately for the three components (Table 2).

| ID | ΔEi (m) | ΔNi (m) | ΔHi (m) | Calculated HRMS (m) | Calculated VRMS (m) |
|---|---|---|---|---|---|
| 1 | 0.015 | 0.041 | 0.029 | 0.043 | 0.029 |
| 2 | -0.008 | 0.019 | 0.024 | 0.021 | 0.024 |
| 3 | 0.004 | 0.025 | 0.031 | 0.026 | 0.031 |
| 4 | 0.057 | 0.012 | 0.029 | 0.058 | 0.029 |
| 5 | 0.035 | 0.036 | 0.027 | 0.050 | 0.027 |
| 6 | -0.024 | 0.026 | 0.059 | 0.035 | 0.059 |
| 7 | 0.050 | 0.044 | 0.019 | 0.066 | 0.019 |
| 8 | 0.007 | 0.036 | 0.004 | 0.037 | 0.004 |
| 9 | 0.016 | -0.002 | 0.032 | 0.016 | 0.032 |
| 10 | -0.029 | 0.073 | 0.035 | 0.079 | 0.035 |
| 11 | -0.036 | 0.026 | 0.005 | 0.045 | 0.005 |
| 12 | -0.001 | 0.087 | -0.032 | 0.087 | 0.032 |
| 13 | -0.003 | 0.068 | 0.017 | 0.068 | 0.017 |
| 14 | -0.053 | 0.048 | 0.000 | 0.071 | 0.000 |
| 15 | -0.019 | 0.070 | -0.031 | 0.072 | 0.031 |
| 16 | 0.013 | 0.023 | 0.011 | 0.026 | 0.011 |
| 17 | 0.045 | 0.024 | 0.030 | 0.051 | 0.030 |
| 18 | 0.059 | 0.031 | 0.027 | 0.067 | 0.027 |
| 19 | 0.016 | 0.064 | 0.018 | 0.066 | 0.018 |
| 20 | 0.012 | 0.042 | 0.036 | 0.043 | 0.036 |

Table 2. GNSS-Ph vs TS comparison

The empirical horizontal and vertical accuracies were summarized by horizontal and vertical root mean square error (HRMSE and VRMSE), computed over all $N$ surveyed points as:

$$HRMSE = \sqrt{\frac{1}{N}\sum_{i=1}^{N}\left(\Delta E_i^2 + \Delta N_i^2\right)} = 0.055 \text{ m}$$

$$VRMSE = \sqrt{\frac{1}{N}\sum_{i=1}^{N}\Delta H_i^2} = 0.027 \text{ m}$$

The mean signed residuals, computed separately for each component, are used to evaluate systematics effects:

Signed mean $\Delta E_i$ = 0.008 m
Signed mean $\Delta N_i$ = 0.040 m
Signed mean $\Delta H_i$ = 0.019 m

After assessing the absolute accuracy of the GNSS measurements through the coordinate residuals and the corresponding horizontal and vertical RMSE metrics, the analysis of inter-point distances was introduced to evaluate the relative geometric consistency of the surveyed point set.

The inter-point distance analysis was performed by computing 190 unique pairwise distances among the 20 surveyed points in both the GNSS and total station datasets, and by comparing the corresponding 3D values in order to quantify the relative geometric consistency of the GNSS survey with respect to the reference measurements.

The results showed that the GNSS-Ph survey produced a mean absolute 3D inter-point discrepancy of 0.038 m and an RMSE of 0.047 m with respect to the TS-derived distances, with a maximum discrepancy of approximately 0.110 m.

### 4.2 SfM processing of the GNSS-Ph data.

The second analysis completed focused on the exploitation of a direct georeferencing approach in the SfM processing of GNSS-acquired images. Those images are geotagged during acquisition and can thus be used for this purpose. A commercial software solution (Agisoft Metashape v.2.2.2) was used to process the acquired images. A consolidated rigorous pipeline for SfM processing was followed for estimating exterior and interior orientation parameters, i.e. image matching and tie points extraction and bundle block adjustment.
All 71 images acquired with the GNSS were successfully aligned; a schematic representation of the camera positions is shown in Figure 7.

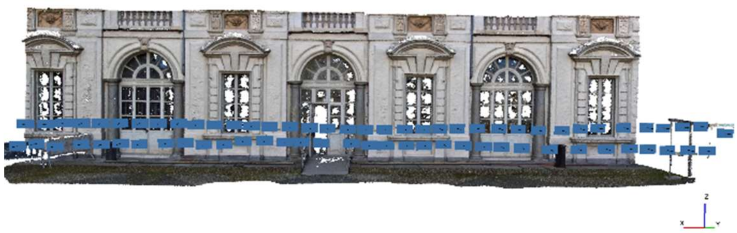

Figure 7. SfM processing of the GNSS acquired images. Scheme of the estimated camera positions.

The ground control points measured with the traditional topographic approach (TS) were used as Check Points (CPs) to evaluate the overall accuracy of the process.

The error on camera location after the processing is reported in Table 3. A brief analysis of the results confirms the overall good performance of the direct georeferencing approach. This evaluation is also confirmed by the global RMS error (RMSE) on the CPs, as reported in Table 4.

| Easting error | Northing error | Vertical error | Planimetric error | 3D Error |
|---|---|---|---|---|
| 0.004 m | 0.017 m | 0.028 m | 0.018 m | 0.034 m |

Table 3. Mean error on camera location after image alignment

| Easting error | Northing error | Vertical error | Planimetric error | 3D Error |
|---|---|---|---|---|
| 0.012 m | 0.017 m | 0.015 m | 0.021 m | 0.026 m |

Table 4. RMSE on 20 CPs

The results reported in the above-mentioned tables are obtained by performing a self-calibration approach to re-estimate the camera's interior orientation parameters.

In our case, it was also useful to evaluate the spatial distribution of the RMSE on the CPs. As shown in Figure 8, the error increases in both the planimetric and altimetric components toward the left side of the façade in the image.


https://doi.org/10.5194/isprs-archives-XLIX-B2-2026-901-2026 | © Author(s) 2026. CC BY 4.0 License.

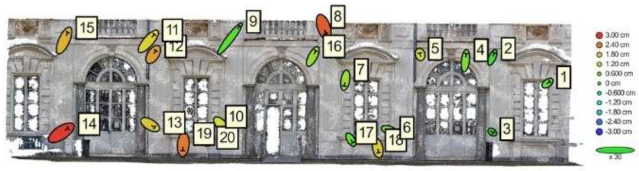


Figure 8. Spatial distribution of RMSe on CPs. Planimetric component is represented by the ellipse shape and size, while altimetric component is represented by mean of colours

This behaviour can likely be attributed to the building configuration. The area affected by bigger errors is the one closer to the main building of the Castello del Valentino that forms a corner near this part of the façade (Figure 3 – Est side of the courtyard). In this area, the surrounding geometry may degrade GNSS performance through partial signal obstruction, reduced satellite visibility, and possible multipath effects, resulting in lower positioning precision.

### 4.3 Added value SfM metric products analysis

The third and final analysis was carried out on the added value metric products that can be generated by adopting an SfM approach using the GNSS-Ph data: point cloud and orthophoto.

A processed and georeferenced LiDAR dataset for the same area of the Castello was available and used as a ground reference for the 3D model analysis. The LiDAR dataset (30 scans) was acquired with a FARO Focus 3D S120.

The data were processed following a consolidated pipeline that integrates cloud-to-cloud (C2C) scans registration via an Iterative Closest Point (ICP) algorithm and georeferencing of the data using measured coded targets.

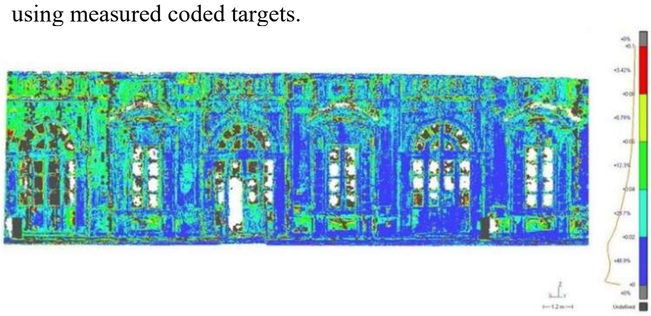

Figure 9. C2C analysis between LiDAR and GNSS-Ph point clouds

The final mean error in the scan registration was 0.004 m, while the error in the target georeferencing was 0.005 m.

A simple C2C analysis was carried out in Cyclone 3DR (v. 19.1.4) between the LiDAR point cloud and the GNSS-Ph one. The threshold for the analysis was set to 0.1 m, and the results are reported in Figure 9 and Table 5.

| GNSS-Ph – Lidar C2C distances | <0.02 m | <0.04 m | <0.06 m | <0.08 m |
|---|---|---|---|---|
| Percentage of points | 49% | 79% | 91% | 97% |

Table 5. C2C Analysis between GNSS-Ph and LiDAR point clouds. Percentage distribution of C2C distances.

The distribution of the distances between the two point clouds highlights the overall good performance of the GNSS-Ph solution. The representation of the spatial distribution, however, confirms what already emerged from the CPs analysis shown in Figure 8. The increase in positional errors on the left part of the façade is also evident on the C2C analysis, as expected.

To further analyse the quality of the 3D model, the point cloud covering the area of the façade was filtered on the basis of the confidence value estimated during the densification process (Figure 10). This parameter is proportional to the number of depth maps that were used to estimate the coordinates of each point of the 3D model. Only points with a confidence parameter greater than 10 were retained in the point cloud, resulting in a 3D model that covers 150 m$^2$ of the façade with reasonable confidence.

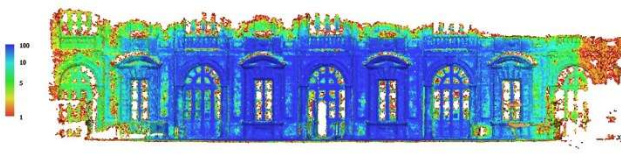

(a)

(b)

Figure 10. False colours representation of the confidence values of the point GNSS-Ph point cloud. Original point cloud (a) and filtered one (b)

For this area, the total number of extracted points is around 1.8 million. Considering the quite low resolution of the camera (2MP with an image size of 1920x1080 pixels), this number can be considered a good result and suitable to describe the overall geometry of the façade.

The quality is, of course, far from the data generated using high quality sensors; nevertheless, it can be of use as a first metrically validated product in several research fields connected to the study and analysis of Built Heritage.

The quality of the point cloud based on the GNSS-Ph approach is shown in Figure 11.

A qualitative analysis of the orthophoto of the façade generated at the end of the SfM processing was also carried out. The orthophoto has a Ground Sample Distance (GSD) of 7 mm/pixel and a general high level of detail.

Figure 11. Example of the level of detail of the 3D point cloud based on the GNSS-Ph approach

Also in this case, this added-value metric product can cover the needs of different application domains related to the built heritage. As it is possible to see in Figure 12, especially in the detail snapshot, the building's architectural details are sharp and well-defined.
Like the point cloud, this product is a dataset that can be rapidly acquired in the field and used to complement the information derived from other datasets.

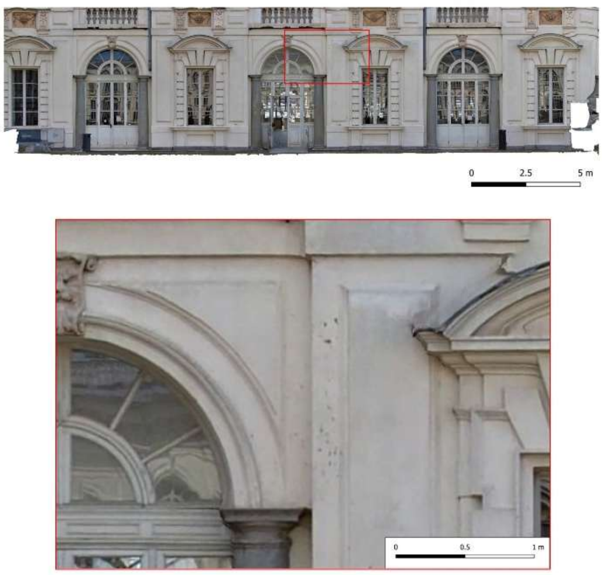


Figure 12. The GNSS-Ph generated orthophoto (top) and an architectural detail.

## 5. Discussion and conclusion

The results of the test reported in this contribution allow us to highlight several points of interest and to outline further research perspectives. The device's declared centimetric accuracy was confirmed by the test, and its possible use in the Built Heritage documentation domain was discussed and evaluated.

In this domain, the lack of resources is often a critical factor and a compromise between acquisition speed, accessibility, and metric accuracy is frequently required. The results reported in this contribution confirm that the GNSS-Ph approach can be successfully deployed across a wide range of applications where sub-decimetric positional accuracy is acceptable.

The results presented in section 4.1 indicate that the GNSS internal quality indicator underestimated the true horizontal error, while the vertical uncertainty estimate was generally consistent and slightly conservative.

The systematic offset was dominated by the northing component, while the easting bias remained limited. This suggests that the horizontal discrepancy was not purely random, but was partly affected by a systematic planimetric shift. This behaviour may be related to satellite geometry at the time of acquisition, local signal obstruction and multipath effects, residual biases in the integration between GNSS positioning and photogrammetric reconstruction, etc. Such systematic effects should be carefully considered when high absolute accuracy is required; nevertheless, in specific application scenarios, their influence might be negligible.

From an application perspective, these findings imply that the GNSS estimates can be considered a good indication of the coordinates accuracy, especially for the vertical component, and both HRMSE and VRMSE are in the centimetric range, in line with the expected accuracy of the employed NRTK service (from the service specification, planimetric accuracy ~2-3 cm and vertical accuracy lower than 5 cm).

In the same section, the inter-point distance analysis shows that even when individual point coordinates fall within the expected nominal accuracy range, the propagation of residual 3D errors between pairs of points may produce relative discrepancies approaching several centimetres and, in the worst cases, about one decimetre. Therefore, the analysis of pairwise 3D distances represents a useful complement to point-wise residual analysis, because it evaluates not only the absolute agreement with the reference system but also the extent to which the surveyed network preserves its internal spatial configuration.

In section 4.2, the spatial distribution of the errors clearly demonstrates the influence of local environmental conditions on the GNSS observations. Areas affected by signal obstruction and multipath effects, such as near building corners, exhibit significant degradation in both planimetric and altimetric accuracy.

From an operational perspective, some limitations of the system emerged during the acquisition phase. The relatively narrow field of view and low camera resolution require short acquisition distances and careful survey geometry planning. These factors might limit the use of these approaches in large or complex architectural scenarios.

Finally, the successful use of the GNSS-acquired images in a Structure from Motion workflow represents a significant added value of the proposed approach. The possibility of using these images within a direct georeferencing approach allows the users to have an additional spatial dataset to generate controlled added value metric products, even if with a lower quality compared to more consolidated approaches.

In terms of geometric quality, the GNSS-Ph approach shows lower geometric fidelity compared with high-resolution LiDAR data, as expected. Nevertheless, the obtained results demonstrate that it can provide a sufficiently accurate representation of the overall geometry, making it suitable for rapid documentation tasks or as a complementary dataset in a multisensor and multiscale approach.

From a practical perspective, the proposed method can significantly reduce fieldwork time and operational complexity, particularly in scenarios where the use of total stations is constrained by accessibility or cost. The ability to measure points on vertical surfaces without physical targets is a major advantage in heritage contexts, where interventions on the object are often limited or prohibited.

Overall, the presented tests show that GNSS-camera-integrated systems have significant potential for Built Heritage documentation, particularly in scenarios where accessibility, acquisition time, and cost-effectiveness are key constraints. Their main strength lies in the ability to measure inaccessible natural points on vertical surfaces and simultaneously acquire georeferenced images that can also be used in SfM workflows.

Future developments should focus on improving the radiometric and geometric quality of the onboard cameras, on exporting full camera orientation parameters to fully exploit direct georeferencing approaches, and on testing the method under different acquisition geometries and environmental conditions, future work will include testing a traditional RTK approach to further improve the accuracy of the measured points.

Within these limits, the proposed workflow can already be considered a promising hybrid solution that bridges traditional topographic surveying and photogrammetric modelling in a practical and operationally efficient way.

## References

Agüera-Vega, F., Carvajal-Ramírez, F., & Martínez-Carricondo, P. (2017). Assessment of photogrammetric mapping accuracy based on variation ground control points number using unmanned aerial vehicle. *Measurement: Journal of the International Measurement Confederation*, *98*(98), 221–227. https://doi.org/10.1016/j.measurement.2016.12.002

Bolkas, D. (2019). Assessment of GCP Number and Separation Distance for Small UAS Surveys with and without GNSS-PPK Positioning. *Journal of Surveying Engineering*, *145*(3), 1–17. https://doi.org/10.1061/(ASCE)SU.1943-5428.0000283

Forlani, G., Dall’Asta, E., Diotri, F., Cella, U. M. di, Roncella, R., & Santise, M. (2018). Quality Assessment of DSMs Produced from UAV Flights Georeferenced with On-Board RTK Positioning. *Remote Sensing*, *10*(2), 311. https://doi.org/10.3390/rs10020311

Rangel, J. M. G., Gonçalves, G. R., & Pérez, J. A. (2018). The impact of number and spatial distribution of GCPs on the positional accuracy of geospatial products derived from low-cost UASs. *International Journal of Remote Sensing*, *39*(21), 7154–7171. https://doi.org/10.1080/01431161.2018.1515508

Remondino, F., & Campana, S. (2014). 3D recording and modelling in archaeology and cultural heritage: Theory and best practices. In *BAR international series 2598* (p. 6). https://doi.org/10.1177/0959683614545031

Seo, D.-M., Woo, H.-J., Hong, W.-H., Seo, H., & Na, W.-J. (2024). Optimization of Number of GCPs and Placement Strategy for UAV-Based Orthophoto Production. *Applied Sciences*, *14*(8). https://doi.org/10.3390/app14083163

Štroner, M., Urban, R., Reindl, T., Seidl, J., & Brouček, J. (2020). Evaluation of the Georeferencing Accuracy of a Photogrammetric Model Using a Quadrocopter with Onboard GNSS RTK. *Sensors*, *20*(8), 2318. https://doi.org/10.3390/s20082318

Teppati Losè, L., Chiabrando, F., & Maschio, P. (2023). DIRECT GEOREFERENCING APPROACHES FOR CLOSE-RANGE AND UAV PHOTOGRAMMETRY IN THE BUILT HERITAGE DOMAIN. *The International Archives of the Photogrammetry, Remote Sensing and Spatial Information Sciences*, *XLVIII-M-2–2023*, 1557–1564. 29th CIPA Symposium “Documenting, Understanding, Preserving Cultural Heritage. Humanities and Digital Technologies for Shaping the Future” - 25–30 June 2023, Florence, Italy. https://doi.org/10.5194/isprs-archives-XLVIII-M-2-2023-1557-2023

Tomaštík, J., Mokroš, M., Surový, P., Grznárová, A., & Merganič, J. (2019). UAV RTK/PPK Method—An Optimal Solution for Mapping Inaccessible Forested Areas? *Remote Sensing*, *11*(6), 721. https://doi.org/10.3390/rs11060721